A Simple Numerical Method for Hydrostatic Incompressible Models with Rigid Lids

VALDIR INNOCENTINI* AND NIVALDO SILVEIRA FERREIRA

Instituto Nacional de Pesquisas Espaciais, SCT, São Paulo, Brazil

ERNESTO DOS SANTOS CAETANO NETO

Instituto de Pesquisas Meteorológicas, UNESP, São Paulo, Brazil

(Manuscript received 15 March 1993, in final form 1 June 1993)

ABSTRACT

A simple and easily implemented method is developed to keep the vertical velocity equal to zero at the bottom and top of hydrostatic incompressible numerical models. The pressure is computed at the top by correcting its value given in the previous time step so that the vertical integral of the horizontal divergence is zero at each column. Numerical experiments that exhibit small time variations of pressure at the top are able to simplify the algorithm and save computer time. Numerical simulations illustrate the method effectiveness for a horizontal deformation-induced frontogenesis.

1. Introduction

Several problems in fluid dynamics require solutions that describe the flow bounded by two rigid lids. In meteorology, many numerical experiments have been designed to maintain vertical velocity zero or nearly zero at the top, attempting to include one tropopause feature without its explicit simulation (Perkey and Kreitzberg 1977; Ballentine 1982; Ross and Orlanski 1982). The control of the vertical velocity at the top usually demands an extra equation for the pressure, which depends on the approach and vertical coordinate adopted, in addition to the primitive equations.

Over complex topography, a normalized terrain-following coordinate has been preferred. Anthes and Warner (1978) describe a hydrostatic numerical model using σ–p coordinate. In this coordinate the compressible continuity equation takes the form of that for incompressible fluids. The surface pressure tendency is derived to satisfy $\omega \equiv dp/dt = 0$ at the top and bottom, and the hydrostatic equation determines the pressure profile from the density. Although the numerical procedure is simple and satisfies the requirement $\omega = 0$ at both boundaries, the upper lid is not rigid.

A type of σ–z coordinate (time independent) is proposed by Ballentine (1982) in a hydrostatic compressible model. He obtains a tendency equation for the pressure at the top so that the vertical velocity is zero at both boundaries. However, the system of equations includes the fast-moving sound waves and requires considerable computer time to solve his Eq. (15).

For a nonhydrostatic compressible flow, an elliptic partial differential equation with the same dimension of the domain must be solved for the pressure. Its finite-difference form with several boundary conditions, including rigid lids, can be found in Harlow and Welch (1965). A discussion on numerical methods usually employed to solve this equation is presented by Meesters (1992).

In many problems a hydrostatic incompressible model can be applied. Its main attractions are the simplicity of the numerical code and the shorter computer time required. In its simpler form, the pressure is prescribed at the top and the profile is obtained by the hydrostatic equation, while the vertical velocity is diagnosticated from the vertically integrated continuity equation using the given bottom velocity.

Ross and Orlanski (1982), hereafter RO, proposed a method to be used in hydrostatic incompressible models that maintains the vertical velocity zero at both boundaries. In fluid problems where the vertical propagation of internal gravity waves is equally important as advective processes, an open lid is more suitable (Klemp and Durran 1984). Here, we merely discuss the RO algorithm and propose a computationally faster and simpler numerical method. Section 2 considers the formulation of the method. Section 3 presents the numerical model and the initial conditions of a horizontal deformation-induced frontogenesis experiment designed to test the effectiveness of the method. Section

* Current affiliation: Instituto de Pesquisas Meteorológicas, UNESP, São Paulo, Brazil.

Corresponding author address: Dr. Valdir Innocentini, Instituto de Pesquisas Espaciais-CPTEC, Av. dos Astronautas, 1758, Caixa Postal 515, 12201-São José dos Campos, São Paulo, Brazil.

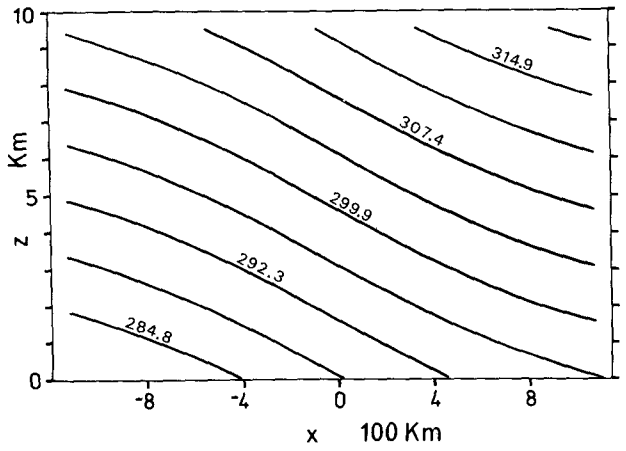

FIG. 1. Initial field of the potential temperature (K) used in experiments E1, E2, E3, and E4. Contour interval is 3.77 K.

4 compares the results using the proposed algorithm and those obtained with the RO method. Finally, the main conclusions are summarized in section 5.

2. Derivation of the method

The RO method may be presented by considering the two-dimensional set of equations consisting of the x-momentum, hydrostatic, and continuity equations, written in terrain-following coordinates:

$$\frac{\partial u}{\partial t} = -\theta \frac{\partial \pi}{\partial x} + F, \tag{1}$$

$$\frac{\partial \pi}{\partial \sigma} = -\frac{gz^*}{\theta}, \tag{2}$$

$$\frac{\partial uz^*}{\partial x} + \frac{\partial \dot{\sigma} z^*}{\partial \sigma} = 0, \tag{3}$$

where

$$\sigma = \frac{z - z_t}{z^*}, \quad z^* = z_s - z_t,$$

z_s and z_t are the surface and top heights, respectively, $\dot{\sigma} \equiv d\sigma/dt$, and π is the Exner function. The term F in (1) represents local sources and/or sinks of x momentum other than the term explicitly indicated. All variables have the usual meaning. The y-momentum and thermodynamic equations should also be considered in order to complete the system, although they are irrelevant in the following discussion. The continuity equation defines the streamfunction ψ by $\partial\psi/\partial\sigma = z^*u$ and $\partial\psi/\partial x = -z^*\dot{\sigma}$.

The foregoing equations can be integrated with three possibilities: (i) a boundary condition for π and other for $\dot{\sigma}$, (ii) two boundary conditions for π, and (iii) two boundary conditions for $\dot{\sigma}$. Alternative (i) integrates the equations the easiest but the vertical velocity can

TABLE 1. Summary of the main characteristic of each numerical experiment.

Experiment	Main characteristic
E1	π_t constant
E2	π_t in geostrophic balance
E3	π_t computed by solving Eq. (8)
E4	π_t computed by solving Eq. (10)

be controlled at only one horizontal boundary. Alternatives (ii) and (iii) permit the control of π and $\dot{\sigma}$ at both boundaries, respectively. The focus of this paper is boundary condition (iii).

Although any numerical time scheme can be adopted to solve (1), we will apply the leapfrog, for simplicity. In this case (1) results in

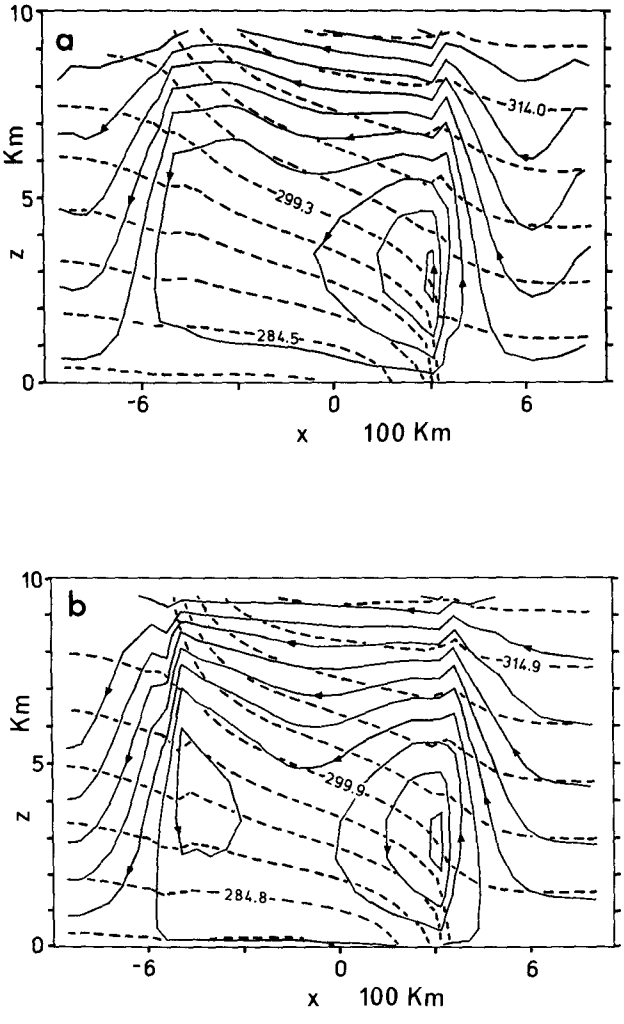

FIG. 2. Streamlines (continuous lines with arrows) and isotherms (broken lines) for experiments (a) E3 and (b) E4. In (a) contour intervals are 5508.1 $m^3 s^{-1}$ and 3.68 K, and in (b) 5694.3 $m^3 s^{-1}$ and 3.77 K.

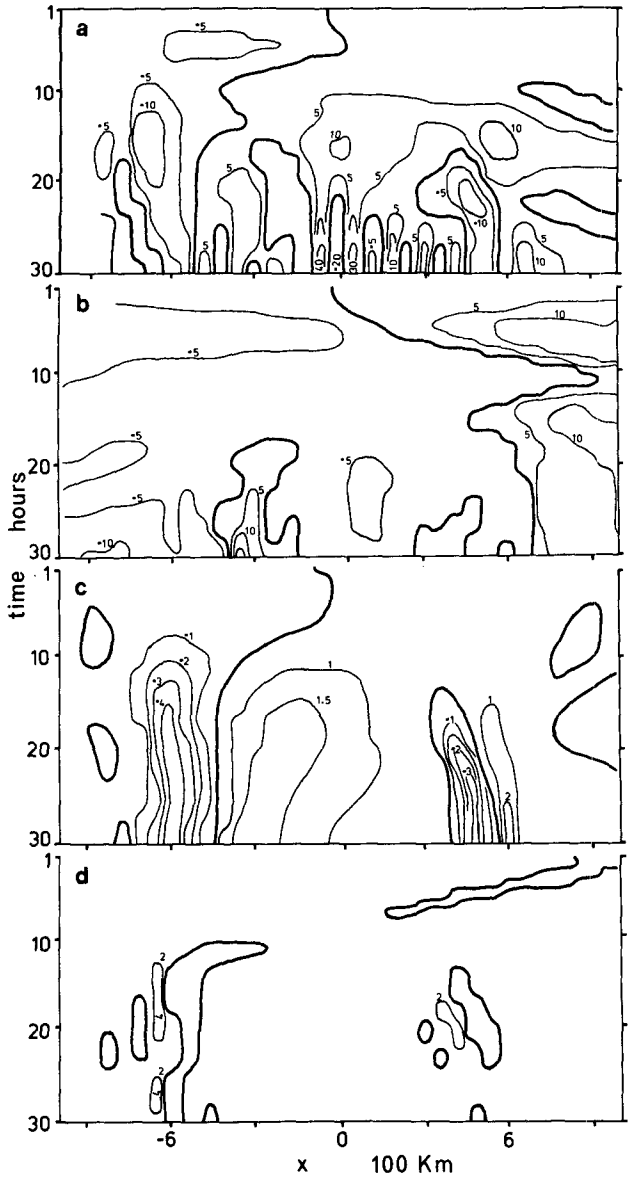

FIG. 3. Vertical velocity at each 1-h interval at the top as a function of x distance for experiments (a) E1, (b) E2, (c) E3 in centimeters per second, and (d) E4 (10^{-2} cm s^{-1}). Heavy continuous lines represent the zero contour.

$$u^{n+1} - u^{n-1} = 2\Delta t\left(-\theta\frac{\partial\pi}{\partial x} + F\right), \tag{4}$$

where the upper index denotes the time level (n on the right-hand side is omitted for simplicity). Multiplying (4) by z^*, applying $\partial/\partial x$, integrating vertically from $\sigma = 0$ to $\sigma = 1$, and using (3), we get

$$\delta(\overline{z^*\mathring{\sigma}^{n+1}}) - \delta(\overline{z^*\mathring{\sigma}^{n-1}}) = 2\Delta t\left[-\frac{\partial}{\partial x}\left(\overline{z^*\theta\frac{\partial\pi}{\partial x}}\right) + \frac{\partial\overline{z^*F}}{\partial x}\right], \tag{5}$$

where δ is the difference of the variable between the levels $\sigma = 1$ and $\sigma = 0$, and the bar denotes the vertical integration. If one wants $\delta\mathring{\sigma}^{n+1} = 0$, then (5) becomes a diagnostic equation for π:

$$\frac{\partial}{\partial x}\left(\overline{z^*\theta\frac{\partial\pi}{\partial x}}\right) = \frac{\partial\overline{z^*F}}{\partial x} + \frac{1}{2\Delta t}\delta(\overline{z^*\mathring{\sigma}^{n-1}}). \tag{6}$$

a. The RO method

Defining the hydrostatic pressure π_h by

$$\pi_h(\sigma) = -\int_0^\sigma \frac{gz^*}{\theta}\,d\sigma', \tag{7}$$

from (2) we have $\pi = \pi_h + \pi_t$, where π_t is the pressure at the top. Then (6) takes the form

$$\frac{\partial}{\partial x}\left(\overline{z^*\theta}\frac{\partial\pi_t}{\partial x}\right) = -\frac{\partial}{\partial x}\left(\overline{z^*\theta\frac{\partial\pi_h}{\partial x}}\right) + \frac{\partial\overline{z^*F}}{\partial x}, \tag{8}$$

where the last term of (6) has been neglected by RO. This assumption seems reasonable if $\delta\mathring{\sigma} = 0$ at the initial time step. The spatial discretization of (8) leads to a tridiagonal matrix that can be solved by triangulating, provided the lateral boundary condition for π_t is specified. Supposing that all variables are known in the time steps n and $(n-1)$, the numerical procedure can be carried out in the following sequence.

(i) Equation (1) provides u^{n+1}. At the same time one can compute the second term of the rhs of (8).

(ii) The values of θ^{n+1} and π_h^{n+1} computed from the thermodynamic equation and (7), respectively, are used to complete the computation of the rhs of (8).

(iii) The value of π_t^{n+1} is obtained by solving (8), thus determining the total pressure.

Note that if $\mathring{\sigma}$ is set to zero at the bottom in every time step, (8) ensures that $\mathring{\sigma}_t^{n+1} - \mathring{\sigma}_t^{n-1} = 0$ ($\mathring{\sigma}_t$ is the vertical velocity at the top), and $\mathring{\sigma}_t = 0$ must be made in the initial field in order to maintain this condition throughout the period of integration. However, if $\mathring{\sigma}_t$ becomes slightly different from zero, this tendency will be present in the forthcoming time steps. This is something to worry about, when one notes that in (8) all the terms should be referred to the same time level and the numerical code implementation is not straightforward due to practical constraints imposed by programming procedures. The second term in the rhs of (8) (namely, Coriolis force, advection, diffusion, and $-g\sigma\partial z^*/\partial x$ related to the horizontal gradient of the topography) is determined using variables from the previous time step n. This may imply in some error, and its accumulation during the time integration may cause a degradation of the rigid-lid conditions. The method proposed here removes this difficulty.

b. The method proposed

Suppose that the pressure π is used to compute u^{n+1} in an arbitrary time step. Thus, we have

$$\frac{\partial \overline{z^* u^{n+1}}}{\partial x} - \frac{\partial \overline{z^* u^{n-1}}}{\partial x} = 2\Delta t \times \left[-\frac{\partial}{\partial x}\left(\overline{z^*\theta}\, \frac{\partial \pi_h}{\partial x} \right) - \frac{\partial}{\partial x}\left(\overline{z^*\theta}\, \frac{\partial \pi_t}{\partial x} \right) + \frac{\partial \overline{z^* F}}{\partial x} \right]. \quad (9)$$

We suggest that the quantity π_t used in the computation of u^{n+1} be corrected so that its new value π_t^{cor} satisfies (9) with the first term equal to zero. Then, π_t^{cor} is given by

$$\frac{\partial}{\partial x}\left(\overline{z^*\theta}\, \frac{\partial \pi_t^{\text{cor}}}{\partial x} \right) = \frac{1}{2\Delta t} \frac{\partial \overline{z^* u^{n+1}}}{\partial x} + \frac{\partial}{\partial x}\left(\overline{z^*\theta}\, \frac{\partial \pi_t}{\partial x} \right), \quad (10)$$

which can be solved similarly to (8). To maintain the balance in the x-momentum equation, the value of u^{n+1} should be evaluated again according to (1) with the corrected pressure gradient force. With $\mathring{\sigma}_s = 0$ at any time step, note that π_t^{cor} implies in $\mathring{\sigma}_t^{n+1} = 0$, while (8) implies in $\mathring{\sigma}_t^{n+1} - \mathring{\sigma}_t^{n-1} = 0$.

Computer time can be saved if π_t^{cor} is considered as π_t^{n+1}, thus avoiding a repeated calculation of u^{n+1}. Although this assumption produces an imbalance in the x-momentum equation, it will not result in significant inaccuracies, provided π_t has a small time variation. It is clear that the computation of π_t^{cor} using (10) is much easier to implement and demands less computational storage than (8). Another advantage is that (10) requires only two vertical integrations, decreasing substantially the accumulated truncation errors. The next two sections present the numerical model, the experiments, and the results discussion.

3. Numerical model and initial conditions

The numerical model is the two-dimensional set (1), (2), and (3), in addition to the thermodynamic and the y-momentum equations. The Euler-backward time scheme, a second-order approximation in the spatial derivative, and the Arakawa C grid (Mesinger and Arakawa 1976) are used. At the bottom and top, nonslip and stress-free boundary conditions are used, respectively. The vertical velocity $\mathring{\sigma}$ is given by (3) integrated from the bottom, where $\mathring{\sigma} = 0$. At the lateral boundaries, the radiational scheme (Orlanski 1976) is employed for the prognostic variables, and for the diagnostic variables, $\mathring{\sigma} = 0$, and π is obtained from the hydrostatic equation. The domain is 2400 km wide with $\Delta x = 60$ km and 10 km high with $\Delta\sigma = 0.1$. The time step is 300 s and the Coriolis parameter is that of $-45°$ latitude. No horizontal diffusion or damping procedure is included (except that implicit in the temporal scheme used), since the main objective here is to emphasize the simplicity and effectiveness of the method proposed. Further details of the numerical model can be found in Innocentini (1986).

The initial conditions are an adaptation from Williams (1972): a steady barotropic horizontal deformation is imposed on a baroclinic field initially in geostrophic balance. They are given by

$$u(x, \sigma, t) = Dx + u'(x, \sigma, t),$$
$$v(x, \sigma, t) = Dy + v'(x, \sigma, t),$$
$$\sigma(x, \sigma, t) = \sigma'(x, \sigma, t),$$
$$\theta(x, \sigma, t) = \theta'(x, \sigma, t),$$
$$\pi(x, \sigma, t) = \pi'(x, \sigma, t),$$

where the primed variables refer to the baroclinic field and $D = 2.5 \times 10^{-5}\ \text{s}^{-1}$ is the deformation constant factor. To balance the steady horizontal deformation, the σ coordinate is used in the form

$$\sigma = \frac{z - z_t - A(x, y)}{z^*},$$

where the function A has the analytical form

$$A(x, y) = -\frac{D^2}{2g}(x^2 - y^2) - \frac{fDxy}{g}.$$

The initial baroclinic field is in hydrostatic balance with θ' given by

$$\theta'(x, \sigma) = \theta_0'(\sigma) + \frac{32}{\pi} \tan^{-1}\left(\frac{2x}{L} - 1 \right),$$

where $\theta_0'(\sigma) = 288 + (2.5 \times 10^{-3})(\sigma z^* + z_t)$ K, $L = 2400$ km, and $-1200\ \text{km} \leq x \leq 1200$ km. This field is shown in Fig. 1. Note that the horizontal potential temperature gradient is constant with height and decreases toward the lateral boundaries.

4. Numerical tests

Four numerical experiments were carried out. Table 1 provides their main characteristics; except for the procedure to obtain π_t, they are exactly the same. In E1 the top pressure is kept constant and equal to the initial value. In E2, after having computed v^{n+1} at the top, π_t^{n+1} is calculated to maintain the geostrophic balance. In both experiments the hydrostatic equation is integrated from the top to the bottom. Experiment E3 uses the method proposed by RO, while E4 employs the one described here. Equations (8) and (10) are derived from the finite differencing that is analogous to the model equations. In solving these equations the top pressure is assumed constant at both upper boundary corners. It must be stressed that in E1 and E2 there is no control on the vertical velocity at the top, and they are included just for comparison.

Figures 2a and 2b show the streamlines and the isotherms for the experiments E3 and E4, respectively,

after a 30-h model integration. Note that both experiments have similar behavior near the surface. The horizontal potential temperature gradient is about 4 K $(30\ \text{km})^{-1}$ at $x \approx 400$ km. The frontogenesis that starts at $x = 0$ km shifts toward the warm sector with a velocity of about 4 m s^{-1}. A direct transversal circulation, with the ascending motion stronger than the descending, is observed. At this time, this circulation presents a maximum ascending (descending) velocity of about 30 cm s^{-1} (12 cm s^{-1}) in both experiments.

The main distinguishable feature between E3 and E4 appears in the high-level frontogenesis. Note that around $x = -600$ km, E3 presents a potential temperature horizontal gradient of about 4 K $(120\ \text{km})^{-1}$ in contrast with that of 4 K $(60\ \text{km})^{-1}$ for E4. Also, the transversal circulation associated with the high-level frontogenesis is better defined in E4. This is a consequence of the fact that E4 has smaller vertical velocity at the top than E3 (as will be shown in the following), enhancing the upper-level frontogenesis.

Figures 3a, 3b, 3c, and 3d present the vertical velocity at the top for E1, E2, E3, and E4 at each 1-h interval, respectively. Experiments E1 and E2 have very high velocities at the top and suggest the development of numerical instability. Experiment E3 should have vertical velocity zero but due to the accumulation of truncation errors and also to the different time levels inherent in the application of (8) as pointed out in section 2, values slightly greater than -4 cm s^{-1} and $+2$ cm s^{-1} are observed. On the other hand, E4 hardly presents vertical velocity larger than 0.04 cm s^{-1}, revealing the superiority of this algorithm in meeting the requirement of nearly zero vertical velocity at the top.

5. Conclusions

A simple scheme is developed for incompressible and hydrostatic numerical models to maintain the vertical velocity zero at the bottom and top of the domain. The pressure is computed at the top by correcting its value given in the previous time step so that the vertical integration of the divergence of the horizontal velocity is zero. Like the method proposed by RO (Ross and Orlanski 1982), it is based on the removal of the mean barotropic divergence in each vertical column. While in RO the difference in the vertical velocity between two alternated time steps is set to zero on the upper lid, in the proposed method the vertical velocity at each time step is exactly zero. The method proposed in this paper decreases the computational cost because it demands fewer vertical integrations and consequently smaller truncation errors.

In numerical experiments exhibiting small time variation of pressure at the top, the method proposed here can be simplified to avoid computing the horizontal velocity twice at each time step. The results of an experiment with a horizontal deformation-induced frontogenesis using the simplified method show vertical velocity at the top two orders of magnitude smaller than that of the RO method.

Although the method suggested is a numerical artifice, it meets more effectively the requirement $\dot{\sigma} = 0$ at the top than the RO method, and is easier to implement.

Acknowledgments. The authors would like to thank Mr. Marco A. Maringolo and Dr. Prakki Satyamurty. They suggested improvements and corrections on an early draft of the manuscript. We also thank IEAv for supplying computer time.

REFERENCES

Anthes, R. A., and T. T. Warner, 1978: Development of hydrodynamic models suitable for air pollution and other mesometeorological studies. *Mon. Wea. Rev.*, **106,** 1045–1078.

Ballentine, R. J., 1982: Numerical simulation of land-breeze-induced snowbands along the western shore of Lake Michigan. *Mon. Wea. Rev.*, **110,** 1544–1553.

Harlow, F. H., and J. E. Welch, 1965: Numerical calculation of time-dependent viscous incompressible flow of fluid with free surface. *Phys. Fluids,* **8,** 2182–2189.

Innocentini, V., 1986: Numerical simulations of moist slantwise convection. Ph.D. dissertation, University of Reading, England, 224 pp.

Klemp, J. B., and D. R. Durran, 1983: An upper boundary condition permitting internal gravity wave radiation in numerical mesoscale models. *Mon. Wea. Rev.*, **111,** 430–444.

Meesters, A., 1992: Feasibility of the direct method to solve the anelastic pressure equation in nonhydrostatic two-dimensional mesoscale models. *Mon. Wea. Rev.*, **120,** 2390–2393.

Mesinger, F., and A. Arakawa, 1976: Numerical methods used in atmospheric models. GARP Publications Series No. 17, 1–64.

Orlanski, I., 1976: A simple boundary condition for unbounded hyperbolic flows. *J. Comput. Phys.*, **21,** 251–269.

Perkey, D. J., and C. W. Kreitzberg, 1976: A time-dependent lateral boundary scheme for limited-area primitive models. *Mon. Wea. Rev.*, **104,** 744–755.

Ross, B. B., and I. Orlanski, 1982: The evolution of an observed cold front. Part I: Numerical simulations. *J. Atmos. Sci.*, **39,** 296–327.

Williams, R. T., 1972: Quasi-geostrophic versus non-geostrophic frontogenesis. *J. Atmos. Sci.*, **29,** 3–10.